Human Molecular Genetics, 2016, Vol. 25, No. 19 4143–4156

doi: 10.1093/hmg/ddw248
Advance Access Publication Date: 27 July 2016
Original Article

ORIGINAL ARTICLE

Neurodevelopmental alterations and seizures developed by mouse model of infantile hypophosphatasia are associated with purinergic signalling deregulation

Álvaro Sebastián-Serrano[1,2], Tobias Engel[3], Laura de Diego-García[1,2], Luis A. Olivos-Oré[6], Marina Arribas-Blázquez[6], Carlos Martínez-Frailes[1,2], Carmen Pérez-Díaz[7], José Luis Millán[5], Antonio R. Artalejo[6], María Teresa Miras-Portugal[1], David C. Henshall[3,4] and Miguel Díaz-Hernández[1,2,*]

[1]Department of Biochemistry and Molecular Biology, Veterinary School, Complutense University of Madrid, Avda. Puerta de Hierro S/N, Madrid, Spain, [2]Instituto de Investigación Sanitaria del Hospital Clínico San Carlos, IdISSC, Madrid, Spain, [3]Department of Physiology & Medical Physics, Royal College of Surgeons in Ireland, Dublin, Ireland, [4]Irish Centre for Fetal and Neonatal Translational Research (INFANT), Cork, Ireland, [5]Sanford Children's Health Research Center, Sanford Burnham Prebys Medical Discovery Institute, La Jolla, California, [6]Department of Toxicology and Pharmacology, Veterinary School, Complutense University of Madrid, Avda. Puerta de Hierro S/N, Madrid, Spain and [7]Department of Medicine and Animal Surgery, Veterinary School, Complutense University of Madrid, Avda. Puerta de Hierro S/N, Madrid, Spain

*To whom correspondence should be addressed at: Miguel Diaz-Hernandez, Department of Biochemistry and Molecular Biology, Veterinary School, Complutense University of Madrid, Avda. Puerta de Hierro S/N, 28040 Madrid, Spain. Tel: +34913944068; Fax: 34913943909; Email address: migueldiaz@ucm.es

Abstract

Hypomorphic mutations in the gene encoding the tissue-nonspecific alkaline phosphatase (TNAP) enzyme, *ALPL* in human or *Akp2* in mice, cause hypophosphatasia (HPP), an inherited metabolic bone disease also characterized by spontaneous seizures. Initially, these seizures were attributed to the impairment of GABAergic neurotransmission caused by altered vitamin B6 (vit-B6) metabolism. However, clinical cases in human newborns and adults whose convulsions are refractory to pro-GABAergic drugs but controlled by the vit-B6 administration, suggest that other factors are involved. Here, to evaluate whether neurodevelopmental alterations are underlying the seizures associated to HPP, we performed morphological and functional characterization of postnatal homozygous TNAP null mice, a model of HPP. These analyses revealed that TNAP deficient mice present an increased proliferation of neural precursors, an altered neuronal morphology, and an augmented neuronal activity. We found that these alterations were associated

Received: May 24, 2016. **Revised:** July 14, 2016. **Accepted:** July 17, 2016

with a partial downregulation of the purinergic P2X7 receptor (P2X7R). Even though deficient P2X7R mice present similar neurodevelopmental alterations, they do not develop neonatal seizures. Accordingly, we found that the additional blockage of P2X7R prevent convulsions and extend the lifespan of mice lacking TNAP. In agreement with these findings, we also found that exogenous administration of ATP or TNAP antagonists induced seizures in adult wild-type mice by activating P2X7R. Finally, our results also indicate that the anticonvulsive effects attributed to vit-B6 may be due to its capacity to block P2X7R. Altogether, these findings suggest that the purinergic signalling regulates the neurodevelopmental alteration and the neonatal seizures associated to HPP.

Introduction

Tissue-nonspecific alkaline phosphatase (TNAP) is one of the four isozymes of alkaline phosphatase (1). TNAP is present in many tissues, being particularly abundant in skeletal, renal tissue, liver and in the central nervous system (2). Hypomorphic mutations in the gene encoding TNAP (*ALPL* in humans and *Akp2 or Alpl* in mice) give rise to hypophosphatasia (HPP) a rare, and sometimes fatal, inborn error of metabolism (3). Clinical symptoms are heterogeneous, being its perinatal variant the most lethal form. The neonatal form of HPP is characterized by an impairment of bone mineralization, respiratory distress and spontaneous seizures ultimately leading to death a few weeks after birth (3). Initial studies in *Akp2* knockout (TNAP-/-) mice, which reproduce the phenotype of infantile HPP, suggested that these epileptic seizures were triggered by a decrease in brain levels of GABA, caused in turn by alterations in metabolism of vitamin B6 (vit-B6) (4–6). Indeed, several studies have described beneficial effects of treating patients with neonatal HPP with pyridoxine (PN) (7,8); and TNAP-deficient mice with pyridoxal (PL) (5,6), the non-phosphorylated forms of vit-B6. However, some patients with neonatal HPP presented neonatal seizures that were unresponsive to various GABA-acting drugs (e.g., benzodiazepines and barbiturates), but they were effectively controlled by PN administration (7,8). In line with these observat ions, accidental overdose of levamisole, a TNAP inhibitor, triggers seizures that are refractory to diazepam or lorazepam (9,10). Interestingly, the widespread use of levamisole as a cocaine adulterant (11) suggests that inhibition of TNAP may be a concomitant mechanism that has favoured the increase of seizures associated with cocaine use (12). These findings suggest that alterations of other not yet-identified molecular mechanisms, independent of GABAergic neurotransmission, may underlie to the seizures triggered by a deficiency of TNAP activity.

During brain development, seizures and neonatal convulsions are thought to induce a variety of developmental defects. These alterations include cell loss, dispersion of dentate gyrus (DG) granule cells, mossy fiber sprouting, dendritic spine loss, neurogenesis with altered dendritic branching, and ectopic placement of newly generated cells (13–15). Combined, these changes can result in an imbalance between excitation and inhibition that ultimately translates into long-lasting increases in neuronal excitability (16).

Recent studies have provided new evidences implicating TNAP in neurodevelopmental processes. So, several groups have reported that TNAP plays a key role in the proliferation and differentiation processes of precursor cells located in neurogenic zones (17,18). On the other hand, its localization in the synaptic cleft in humans (19) also suggests the involvement of this enzyme in the establishment and maintenance of synaptic contacts (20). Based on the capacity of TNAP to hydrolyze extracellular nucleotides to yield adenosine, this enzyme is proposed as a regulatory element of purinergic signalling in the synaptic cleft (21–23). In this regard, presynaptic TNAP has been reported to favour axonal growth, reducing the availability of adenosine 5′-triphosphate (ATP) around the growth cone by preventing the activation of P2X7 receptor (P2X7R), a member of the ionotropic P2X receptors (24). The P2X7R is widely expressed in the different cellular lineages that shape the brain tissue (21,25) as well as in neural precursors, where it regulates their proliferation (26). In neurons, P2X7R also participates in different physiological events such as the branching of axonal and neurite-like processes (24,27), neurotransmitter release and synaptic plasticity (28,29). In rat hippocampal and midbrain slices, stimulation of P2X7R by selective agonist BzATP elicits an increase in the frequency of spontaneous excitatory postsynaptic currents (sEPSCs) and miniature (m) EPSCs, consequently increasing the excitability of those neurons (30,31). Indeed, the administration of selective and synthetic antagonists of P2X7R reduces seizures and cell death evoked by Kainic acid (KA) in adult and neonatal rodents (32,33). In this regard, it is noteworthy that a recent study has reported that pyridoxal phosphate (PLP), a vit-B6 form, can block, among others P2X receptors, the P2X7R (34).

Here, we explored the role of TNAP and P2X7R in the postnatal brain development and the P2X7R influence in the seizures induced by the absence or inhibition of TNAP.

Results

TNAP is involved in neocortical and hippocampal neuronal development

We first investigated whether TNAP-/- mice display alterations in axonal and dendritic development that could underlie their vulnerability to seizures. We focused on the corpus callosum because in the early postnatal stage, high levels of TNAP are expressed in this structure, through which callosal axons from upper layers grow towards the midline (Figure 1A) . Axonal elongation was evaluated by *in utero* electroporation of EGFP, which can be used to follow the growth of a bundle of axons from a discrete group of neurons. On postnatal day (P) 1, the callosal axonal projections of TNAP-/- mice were shorter (79.3 ± 4.7%) than those of wild type (WT) littermates (Figure 1B and C). Interestingly, although TNAP-/- mice showed a lower cerebral ecto-ATPase activity than WT mice because the absence of TNAP was not compensated by other ectonucleotidases (Supplementary Material, Fig. S1A and B), they did not show any appreciable morphological abnormalities in neocortical cytoarchitecture (Supplementary Material, Fig. S1C). In addition, although these mice showed smaller body size than their respective WT littermates, they did not show an abnormal proportion of the skull size (35).

To analyse dendritic development, we next infected WT and TNAP-/-mice at embryonic day (E) 14.5 with retroviruses expressing EGFP. Considering the perinatal lethality of TNAP-/- mice, we could only analyse neurons from P9 mice. Compared with WT littermates, the neocortical upper pyramidal neurons of TNAP-/- mice had fewer spines, and more secondary dendrites (Figure 1D–F). Similar results were obtained for hippocampal granule

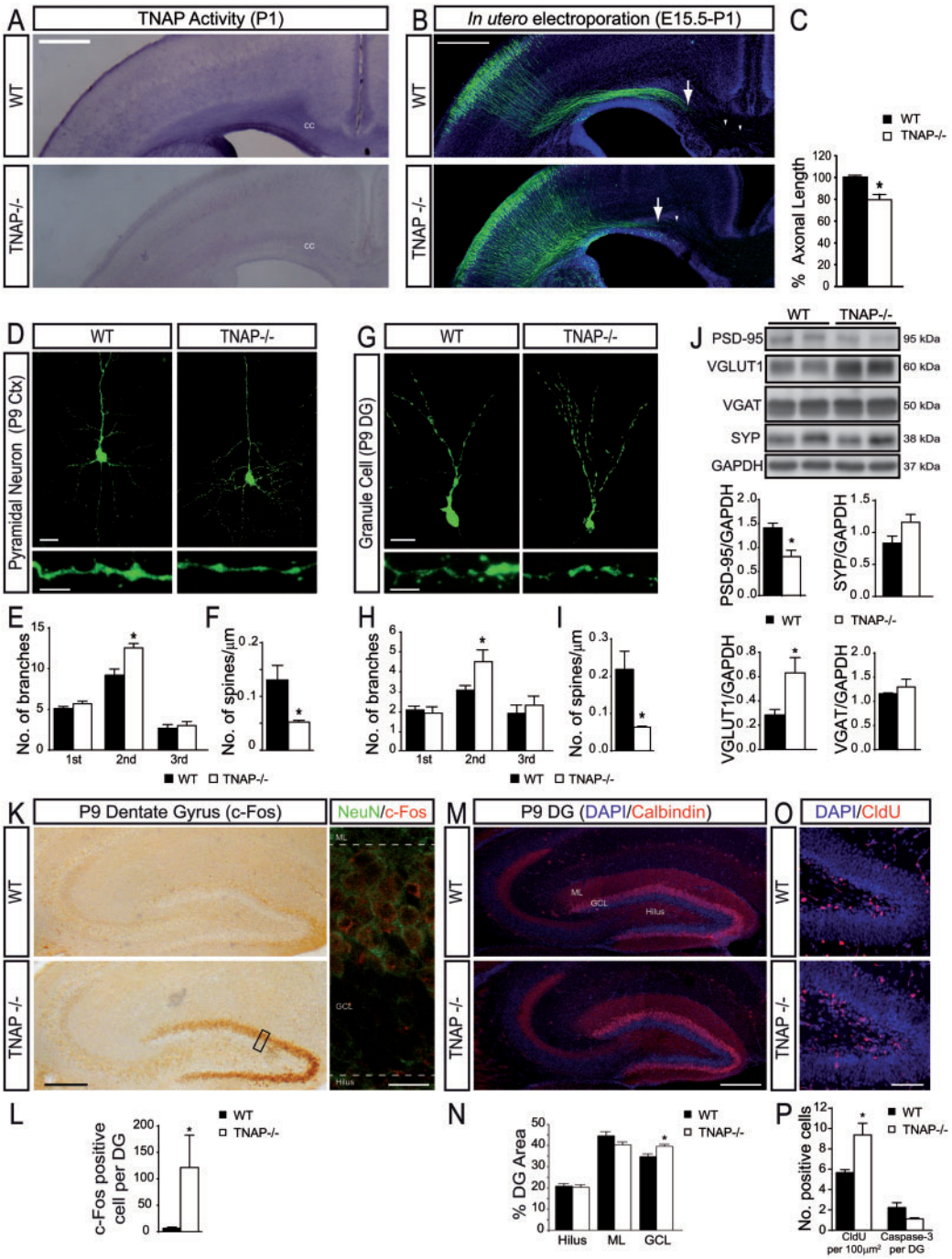

Figure 1. TNAP regulates different events of neocortical and hippocampal neuronal differentiation and proliferation. (**A**) TNAP enzymatic assays on brain slices shows the absence of alkaline phosphatase activity in TNAP-/- mice. cc, corpus callosum. Scale bar: 500 µm. (**B**) Axonal processes from WT or TNAP-/- neocortical neurons electroporated with EGFP can be seen extending medially toward the midline. Arrows indicate the end of the axonal tract and arrowheads point to longer single axons. Scale bar: 500 µm. (**C**) Quantification of axonal length *in vivo* ($n \geq 4$ mice at P1 per genotype; axons ≥200 per mouse). (**D-I**) Representative pictures showing neurons from P9 mice (D) from upper cortical layers or granule cells (G) from dentate gyrus infected by EGFP-expressing retroviruses. Scale bar: 25 µm (upper panels) and 1 µm (lower panels). Total number of primary, secondary, and tertiary branches per neuron in layers II-III (E) or granule cell layer (H). Dendritic spine density in pyramidal neurons (F) or granule cells (I) ($n \geq 3$ mice at P9 per genotype; neurons ≥30 per mouse). (**J**) Representative western blot using samples from hippocampus of P9 WT and TNAP-/- mice. Quantification of the protein expression of PSD-95, VGLUT1, VGAT and SYP ($n \geq 4$ mice at P9 per genotype). (**K**) Micrographs showing increased c-Fos immunoreactivity in the dentate gyrus of TNAP-/- mice compared with WT (left panels). Cells expressing c-Fos in TNAP -/- mice are mainly NeuN positive mature neurons (right panels) Scale bar: 250 µm left panels and 20 µm right panels. (**L**) Total number of c-Fos positive cells in granule cell layer ($n \geq 3$ mice at P9 per genotype; sections ≥10 per mouse). (**M**) Sagittal sections of hippocampus from WT and TNAP-/- mice stained with antibodies against calbindin and DAPI dye to delimit the main layers of the dentate gyrus. Molecular Layer, Granule Cell Layer and Hilus. Scale bar: 200 µm. (**N**) Quantification of the size of different dentate gyrus layers ($n \geq 6$ mice at P9 per genotype; sections ≥10 per mouse) (**O**) Representative micrographs of hippocampal sections of P9 WT and TNAP-/- mice immunostained with anti-CldU antibody after injection with CldU at P6. Scale bar: 100 µm. (**P**) Total number of cells labelled by CldU or Caspase-3 in GCL ($n \geq 3$ mice at P9 per genotype; sections ≥8 per mouse). *$P < 0.05$ between WT and TNAP-/- using unpaired *t* test. Data in bar graphs depict mean ± s.e.m. ML, Molecular Layer. GCL, Granule Cell Layer. DG, Dentate Gyrus. Ctx, cerebral cortex.

cells, which showed reduced dendritic spine number (28.6 ± 4.8% relative to WT) and an increase in secondary dendrites (132.8 ± 19.7% relative to WT) in TNAP-/- versus WT mice (Figure 1G–I). This higher dendrite complexity linked to spine absence could be related to the seizures suffered by TNAP-/- mice. In agreement with the reduction in spines, TNAP-/- mice showed a significant reduction in the postsynaptic density marker PSD-95 at P9 (58.6 ± 9.3% relative to WT) (Figure 1J). Additional biochemical analyses of these mice revealed no alterations in hippocampal levels of the presynaptic markers synaptophysin (SYP) or the vesicular GABAergic transporter (VGAT), but detected a robust increase in the expression of the vesicular glutamatergic transporter 1 (VGLUT1) (Figure 1J). Consistent with an imbalance between excitatory and inhibitory synaptic development, we found high levels of the immediate early gene and neuronal activity marker c-Fos only in TNAP-/- mice (Figure 1K and L). The increased expression of c-Fos was mainly detected in mature neurons from the upper layer of granule cell layer (GCL), which already express the neuronal NeuN marker (Figure 1K, right panel). We also observed in TNAP-/- mice a significant increase in the thickness of GCL of the DG (Figure 1M and N). Since the subgranular cell layer of DG is a site of neurogenesis, we next investigated whether stem cell proliferation was altered. Pulse-chase studies performed using injections of the thymidine analogue 5-Chloro-2′-deoxyuridine (CldU) confirmed a significant increase in neural precursor proliferation in TNAP-/- versus WT mice. However, we did not detect a significant cell death in the hippocampus of these mice (Figure 1O and P). Altogether, these experiments demonstrate that TNAP-/- mice develop alterations in proliferation and neuronal morphology in the neocortex and hippocampus as well as an increased neuronal activity.

TNAP regulates P2X7R expression and function

The absence of TNAP may increase extracellular availability of extracellular ATP, which in turn activates purinergic receptors, including P2X7R. Since it has been reported that TNAP regulates the axonal growth and neuritogenesis by restricting the availability of ATP in the environment of P2X7R (24), we explored this as a potential mechanism underlying the alterations detected in TNAP-/- mice. To address this question we measured P2X7R levels at different postnatal stages in both WT and TNAP-/- mice. While no significant differences between genotypes were detected at P3, P9 TNAP-/- mice showed a significant decrease in hippocampal levels of P2X7R protein (63.9 ± 5.9% relative to WT) and mRNA (40.0 ± 9.9% relative to WT) (Figure 2A and B). A similar reduction was detected in neocortical levels of P2X7R protein (Supplementary Material, Fig. S2A). Despite this decrease, no significant alteration in the receptor distribution pattern was observed in either the neocortex or the hippocampus (Supplementary Material, Fig. S2B). It is noteworthy that reductions in P2X7R were in parallel with the reversal of deficient expression of the presynaptic marker syntaxin (STX) that was initially detected in P3 TNAP-/- mice (Figure 2A).

To allow us to track the effect of TNAP deficiency on P2X7R expression, we crossbred TNAP-/- animals with transgenic mice expressing EGFP under the control of the P2X7R promoter (^{P2X7}EGFP) (Supplementary Material, Fig. S3A). Analysis of these ^{P2X7}EGFP; TNAP-/- mice revealed a significantly reduced numbers of EGFP-positive cells in the DG as compared with ^{P2X7}EGFP control mice (Figure 2C and D). These data indicate that the absence of TNAP results in reduced transcription of the P2X7R. The reduction was equally observed in mature and immature neurons (Figure 2E and F). To determine whether the reduction in P2X7R transcription was accompanied by a decrease in receptor function, we performed patch clamp experiments. Sagittal brain sections from ^{P2X7}EGFP;TNAP-/- and ^{P2X7}EGFP control mice were collected at P9, and EGFP-positive neurons from the Dentate Gyrus (NDG) were stimulated with BzATP (100 μM) in the absence or the presence of the specific P2X7R antagonist A-438079 (10 μM). In all EGFP-positive cells analysed, BzATP gave rise to inwardly-directed non-desensitizing currents that were reversibly blocked by A-438079 (Figure 2G). It is noteworthy that while the mean amplitude of BzATP-induced currents recorded from the soma of the NDG from ^{P2X7}EGFP mice was 47.6 ± 0.7 pA, in cells from ^{P2X7}EGFP; TNAP-/- mice was of 0.6 ± 0.5 pA. These data demonstrate that TNAP deletion largely abolishes the expression of functional P2X7R in the somatic compartment of the NDG (Figure 2H and I).

Given the predominantly presynaptic location of P2X7R (Figure 2J), we next evaluated the functionality of P2X7R at this location. Immunofluorescence and microfluorimetric studies performed with synaptosomes revealed a significant reduction in the number of P2X7R-expressing hippocampal nerve terminals that correlates with a decrease in the number of synaptic terminals that responded to 600 μM ATP in TNAP-/- mice when compared with WT controls (Figure 2K–M). However, these responses were similar in magnitude in both genotypes (Figure 2K). These results demonstrate that TNAP-/- mice develop a higher reduction of P2X7R in the soma than in nerve endings of hippocampal neurons.

P2X7R contributes to altered neuronal development in TNAP-deficient mice

Having established that alterations in neuronal development in TNAP-/- mice are paralleled by decreases in P2X7R expression, we investigated a possible causative link. We first investigated the role of P2X7R in the abnormal axonal growth in TNAP-/- mice. P2X7R were present in callosal projections of these mice (Supplementary Material, Fig. S2C) and we found that selective knockdown of P2X7R by *in utero* electroporation of specific shRNA rescued the decreased axonal growth detected in TNAP-/- mice (Figure 3A and B).

We next sought to determine whether the increase in neural precursor proliferation detected in TNAP-/- mice was also linked to decreased P2X7R expression. To this end, both TNAP-/- mice and WT littermates were treated with the selective P2X7R antagonist Brilliant Blue G, BBG (45.5 mg/kg, i.p.) or with vehicle solution every 48 hours for the first 9 days of life. This antagonist was chosen for *in vivo* studies because it is a slowly reversible P2X7R antagonist (27), permitting a reduced dosing regimen. To monitor the proliferation of hippocampal neural precursors all mice were treated intraperitoneally with CldU (Figure 3C–E). In WT mice BBG treatment increased the number of CldU-positive cells and GCL thickness (Figure 3D and G). By contrast, no significant differences in the number of CldU-positive cells or in GCL thickness were observed between vehicle- and BBG-treated TNAP-/- mice (Figure 3D and G). Analysis of the distribution pattern of CldU-positive cells in BBG-treated mice revealed that, in both ge notypes, these cells spread further into the GCL (reaching the upper layers) than observed in corresponding vehicle-treated controls (Figure 3C and E). Moreover, further analysis of the cytoarchitecture of the DG revealed that pharmacological inhibition of P2X7R resulted in a significant decrease in hilus area, and there was also an increase in the densely packed CA3 pyramidal layer proximal to the DG (CA3pDG) (Figure 3F–H). Immunohistochemical analyses showed that the expansion of CA3pDG was coupled with an increase in the number of axons that are

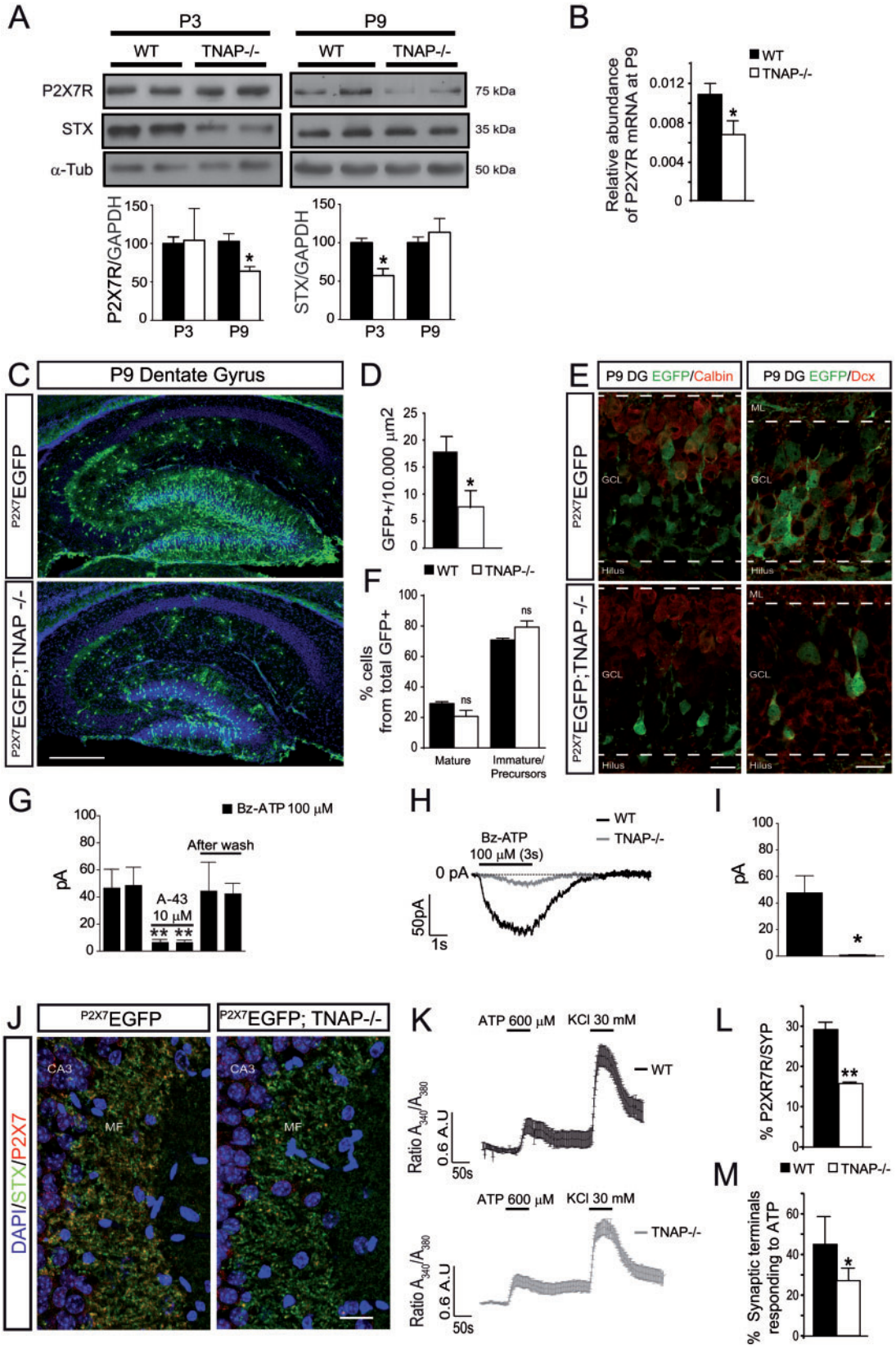

Figure 2. TNAP-/- mice present reduced expression and functionality of hippocampal P2X7R. (**A**) Representative images of western blot using hippocampal samples from P3 and P9 WT and TNAP-/- mice. Graphs show quantification of the protein expression of P2X7R and syntaxin ($n \geq 4$ mice per genotype at each age indicated). (**B**) Quantification of relative abundance of P2X7R mRNA from P9 hippocampus of WT and TNAP-/- mice ($n \geq 4$ mice per genotype). (**C**) Representative micrographs of P9 hippocampal sections from mice expressing EGFP under the P2X7R promoter in the presence (^{P2X7}EGFP) or absence of TNAP-/- (^{P2X7}EGFP; TNAP-/-). Scale bar: 300 µm.

intercalated among the nuclei of CA3pDG (Figure 3F). These axons were projected by granule cells from DG.

Biochemical analyses of BBG-treated TNAP-/- mice revealed that pharmacological inhibition of P2X7R significantly reduced VGLUT1 levels but did not modify the levels of VGAT nor PSD-95 levels (Figure 3I). Finally, we also observed that the treatment with BBG reverted the increased in the number of c-Fos positive cells that was previously observed in the DG from non-treated TNAP-/- mice (Figure 3J and K).

The absence of the P2X7R phenocopies the alterations in neuronal development seen in TNAP-/- mice

Since many of the morphological changes observed in TNAP-/- mice were associated with reduced P2X7R expression and function, we sought to determine whether similar alterations occur in deficient P2X7R (P2X7R-/-) mice. Although P2X7R -/- mice did not develop appreciable epileptic seizures, they show a GCL thicker than in age-matched WT mice at P9 (Fig 4A and B), in a similar way as previously detected in TNAP-/- mice at this state. Furthermore, P2X7R-/- mice also displayed a significant increase in the thickness of the CA3pDG layer (177.3 ± 9.1%) and an attendant reduction in the hilus area (Figure 4A–C). Again, this expansion of CA3pDG was associated with a clear invasion of axonal fibers intercalated among the nuclei of the CA3pDG layer (Figure 4A, right-hand panels). Using injections of CldU into P2X7R-/- mice, we found that the thickening of the GCL was associated with an increase in the proliferation ratio of hippocampal neural precursor cells (183.7 ± 16.6%), which also exhibited greater dispersion within the GCL (Figure 4D–F).

We next used retroviruses expressing EGFP to compare the morphological characteristics of granule cells from DG in P2X7R-/- and TNAP-/- mice. As described above for TNAP-/- mice, the granule cells of P2X7R-/- mice showed an increased number of secondary dendrites with respect to WT controls (155.7 ± 38.7% relative to WT), with a significant reduction in the number of spines (Figure 4G–I). PSD-95 levels were also significantly decreased in P2X7R-/- mice (60.7 ± 8.6% relative to WT) (Figure 4J). At a biochemical level, we found that P2X7R deficient mice showed a significant reduction in VGLUT1 levels but not in VGAT levels, with respect to WT mice (Figure 4J). These data evidence that P2X7R-/- mice present similar alterations that those detected in TNAP-/- mice.

Selective deletion and pharmacological inhibition of P2X7R increases the longevity of TNAP-/- mice: effect of vit-B6 on currents induced by P2X7R activation

To investigate the possible beneficial effect of P2X7R blockage, we quantified longevity in the double transgenic mice lacking both TNAP and P2X7R (Supplementary Material, Fig. S3B) and in TNAP-/- mice treated with the P2X7R antagonist BBG. Double TNAP-/-; P2X7R-/- mice showed a significant increase in longevity, reaching a life expectancy of 12.75 ± 0.7 days of life versus the 9.8 ± 1.0 days of TNAP-/- mice (Figure 5A). Similarly, BBG treatment also increased longevity of TNAP-/- mice up to 14.5 ± 0.6 days. It is also noteworthy that we did not observe, neither in TNAP-/- mice treated with BBG nor in double TNAP-/-; P2X7R-/- mice, the spontaneous seizures that began to be observed in TNAP-/- mice around P6 and characterized by tonic-clonic extension or twisting of their trunk (6)

Vit-B6 has been reported to increase longevity and ameliorate epileptic seizures in TNAP-/- mice (5,6). To assess the potential role of P2X7R in this effect, we again measured currents induced by 100 μM BzATP in EGFP-positive NDG from ^{P2X7}EGFP mice at P9 in the absence or the presence of the two main forms of vit-B6, pyridoxal 5′-phosphate (PLP, 300 μM) and pyridoxal (PL, 300 μM). Interestingly, PLP application reduced by 55.28 ± 9.63% the amplitude of BzATP-induced currents, although PL treatment had no significant effect on currents elicited by BzATP (Figure 5B and C).

Impaired TNAP activity or increase of extracellular ATP triggers seizures via P2X7R activation

Finally, we explored the involvement of the P2X7R in the seizure phenotype in TNAP-deficient mice. Due to perinatal lethality of TNAP-/- mice, it was necessary to perform the *in vivo* electroencephalography (EEG) work using TNAP+/- mice and provoke seizure activity by intracerebroventricular (i.c.v.) injection of ATP to simulate the presumed elevated extracellular ATP in the knockout animals. Initially, we evaluated if TNAP+/- mice presented altered P2X7R expression levels that their WT littermates. We did not observe significant differences in P2X7R expression between TNAP +/- mice and WT littermates at neonatal or adult stages (Supplementary Material, Fig. S4A and B). Moreover, we also found no significant differences in the levels of VGLUT1, VGAT, PSD-95 or SYP between TNAP+/- and WT mice at adult age (Supplementary Material, Fig. S4B). I.c.v. administration of exogenous ATP (18 mg/kg) induced seizures in a comparable proportion of WT and TNAP+/- mice, although the seizure duration was longer in TNAP+/- versus WT mice (67.5 ± 36.8 sec versus 21.2 ± 9.8 sec, respectively) (Figure 6A–C). I.c.v. administration of the selective TNAP antagonists, levamisole (2.4 mg/kg) or SBI-425 (1.2 mg/kg), also elicited seizures in mice of both genotypes (Figure 6E–G and Supplementary Material, Fig. S4C). Interestingly, TNAP+/- mice were more sensitive to levamisole administration than their WT counterparts (70.0% of TNAP+/- treated with levamisole mice had seizures versus 16.6% of WT treated with TNAP antagonist) (Figure 6E–G), but only

(**D**) Quantification of EGFP positive cells from granule cell layer in ^{P2X7}EGFP and ^{P2X7}EGFP; TNAP-/- mice ($n \geq 6$ mice at P9 per genotype; sections ≥10 per mouse). (**E**) Double immunostaining against EGFP (under P2X7 promoter) in green and mature (Calbindin) or immature (Doublecortin, Dcx) neurons in red. Scale bar: 25 μm. (**F**) Graph showing similar reduction of reporter EGFP expression in mature and immature neurons in the absence of TNAP ($n \geq 3$ mice at P9 per genotype, sections ≥4 per mouse). (**G**) Effect of the selective P2X7R antagonist A-438079 (10 μM) on Bz-ATP-induced currents in EGFP-positive neurons situated in the dentate gyrus of WT ($n \geq 12$ cells) and TNAP-/- mice ($n \geq 5$ cells). (**H**) Representative patch-clamp recordings of currents elicited by Bz-ATP (100 μM) in EGFP-positive neurons situated in the dentate gyrus of ^{P2X7}EGFP or ^{P2X7}EGFP; TNAP-/- mice. (**I**) Graph indicates the quantification of patch-clamp recordings showing a significant decrease in the response to Bz-ATP in TNAP-/-mice ($n \geq 7$ cells) compared with WT ($n \geq 12$ cells). (**J**) Representative pictures showing hippocampal mossy fibers from WT and TNAP-/- mice stained with antibodies against P2X7R (red) and syntaxin (green). Scale bar: 25 μm. (**K**) Responses to 600 μM ATP in isolated hippocampal synaptic terminal from P9 WT and TNAP-/- mice. Synaptosomes were stimulated with a pulse of 30 mM KCl at the end of the experiment to assess the functionality of the synaptosomes ($n \geq 3$ mice at P9 per genotype, synaptosomes ≥100 per mouse). (**L**) TNAP-/- mice present a significant decrease in the percentage of hippocampal synaptic terminal expressing P2X7R that correlates with (**M**) a significant decrease in the percentage of synaptic terminals responding to ATP ($n \geq 3$ mice at P9 per genotype, synaptosomes ≥100 per mouse). ns, non-significant, $^{*}P < 0.05$ and $^{**}P < 0.01$ between WT and TNAP-/- using unpaired *t* test. Data in bar graphs depict mean ± s.e.m. ML, Molecular layer. GCL, Granule Cell Layer. MF, Mossy Fibers. DG, Dentate Gyrus.

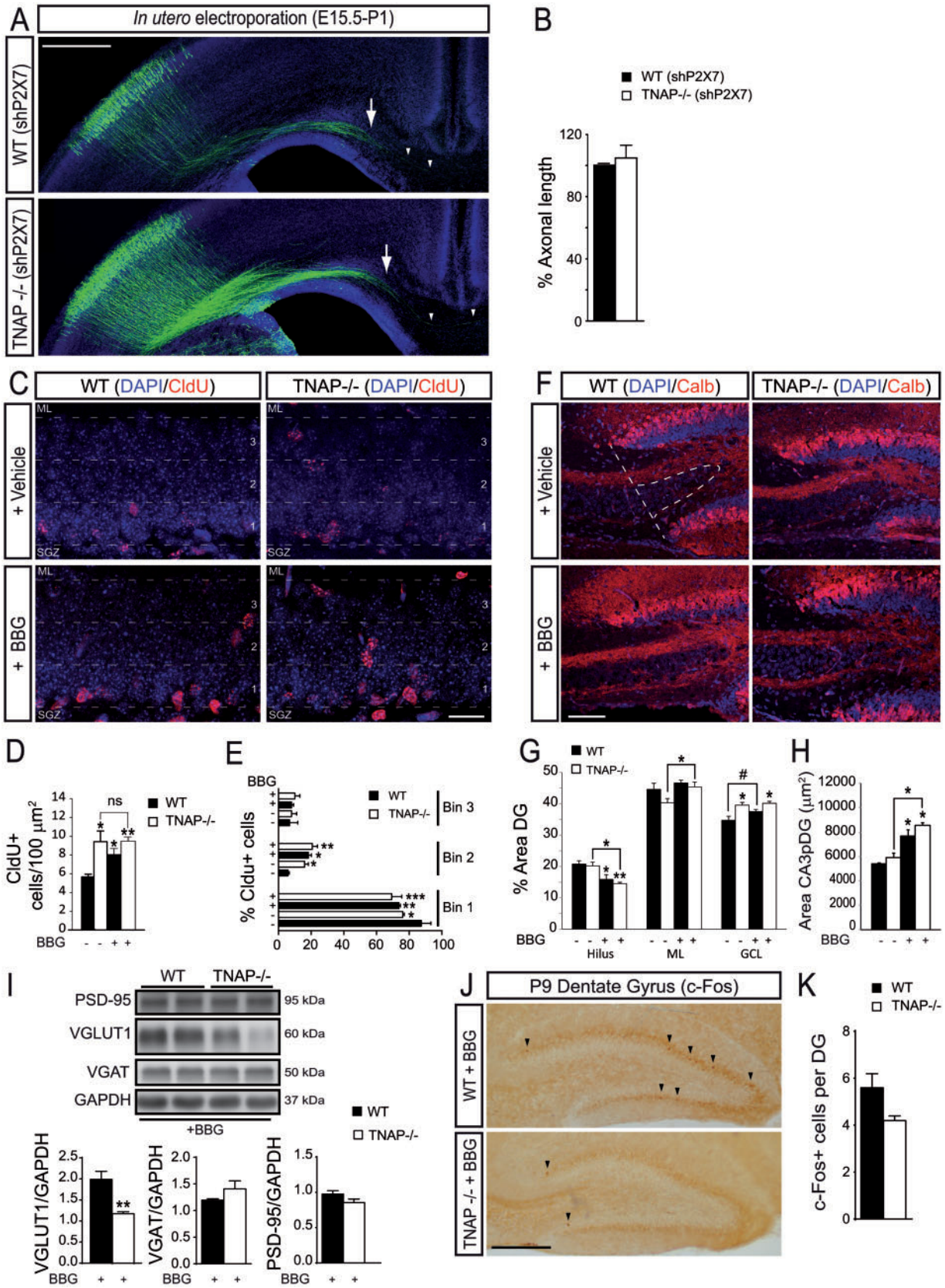

Figure 3. P2X7R is involved in the altered neurodevelopment detected in neonatal TNAP-/- mice. (**A**) Axonal processes from WT or TNAP-/- cortical neurons were co-electroporated with EGFP and shRNA P2X7. Arrows indicate the end of the main axonal tract and arrowheads point to longer single axons. Scale bar: 500 µm. (**B**) Quantification of axonal length *in vivo* ($n \geq 3$ mice at P1 per genotype and axons ≥200 per mouse). (**C**) Representative micrographs of granule cell layer from P9

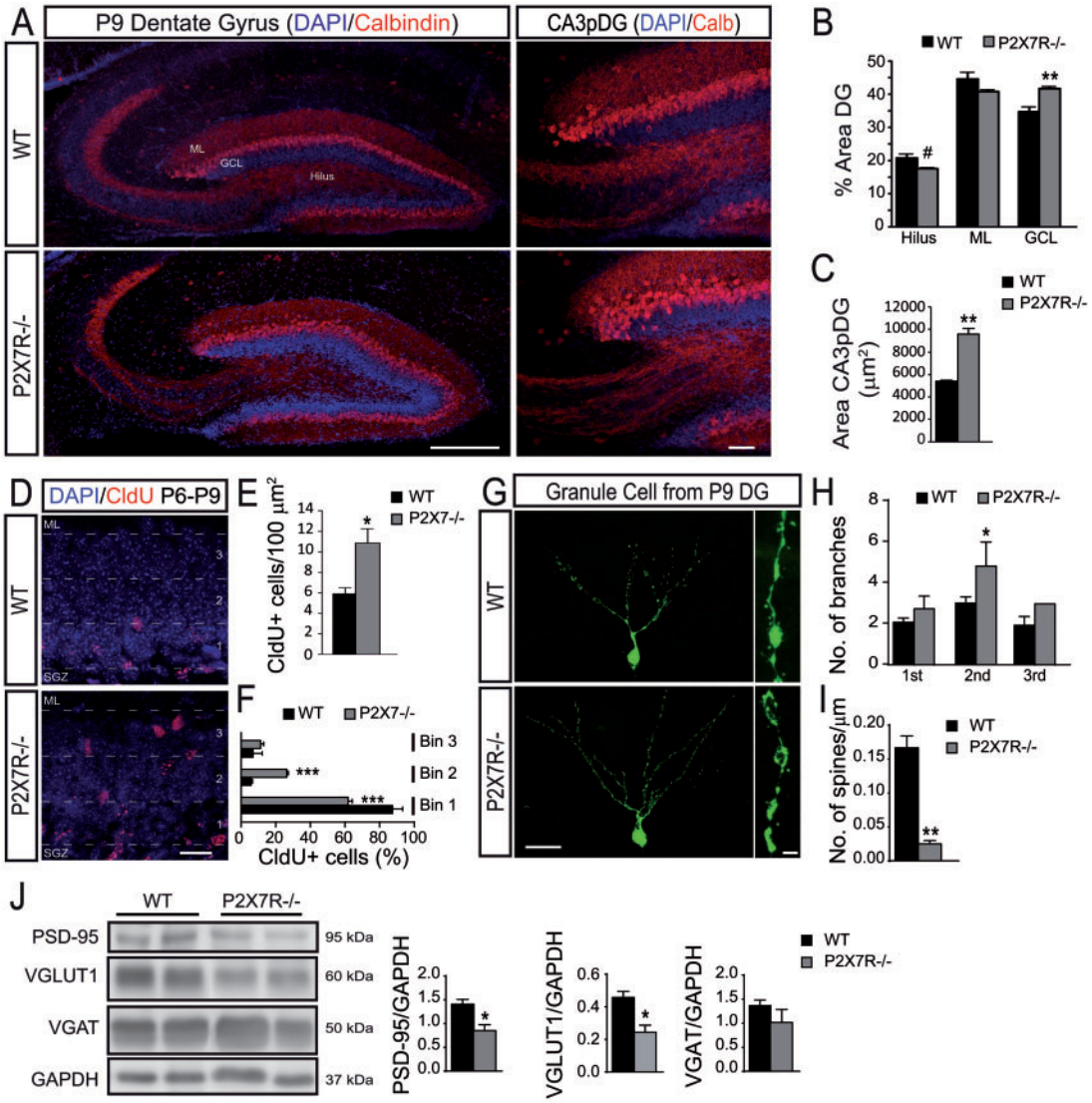

Figure 4. P2X7R-/- mice mimics the neuronal differentiation alterations developed by TNAP-/- mice. (**A**) Representative images of hippocampal sagittal sections from P9 WT and P2X7R-/- mice stained with antibody against Calbindin (red) and DAPI dye (blue) showing dentate gyrus (left panels) and CA3 pyramidal layer proximal to the dentate gyrus (CA3pDG) area (right panels). Scale bar: 200 µm (left panels) and 50 µm (right panels). (**B**) Quantification of the size of different dentate gyrus layers ($n \geq 4$ mice at P9 per genotype; sections ≥10 per mouse). (**C**) Quantification of the size of CA3pDG area ($n \geq 4$ mice at P9 per genotype; sections ≥10 per mouse). (**D**) Representative micrographs of granule cell layer from P9 hippocampal sections showing cells labelled by CldU injections at P6 in WT and P2X7R-/- mice. Scale bar: 20 µm. (**E**) Total number of cells labelled by CldU ($n \geq 3$ mice at P9 per genotype; sections ≥18 per mouse). (**F**) The granule cell layer was divided in 3 equal-sized regions or bins to make quantitative analysis of the distribution of CldU populations ($n \geq 3$ mice at P9 per genotype; sections ≥8 per mouse). (**G**) Representative pictures showing retrovirus labelled granule cells from P9 mice. Scale bar: 25 µm (left panels) and 1 µm (right panels). (**H**) Total number of primary, secondary, and tertiary branches per granule cell ($n \geq 3$ mice at P9 per genotype) (**I**) Dendritic spine density ($n \geq 3$ mice at P9 per genotype; neurons ≥30 per mouse). (**J**) Representative images of western blot using hippocampal samples from P9 WT and P2X7R-/- mice. Quantification of the protein expression of PSD-95, VGLUT1 and VGAT ($n \geq 4$ mice at P9 per genotype). #$P < 0.06$, *$P < 0.05$, **$P < 0.01$ and ***$P < 0.001$ between WT and P2X7R using unpaired *t* test. Data in bar graphs depict mean ± s.e.m. ML, Molecular layer. GCL, Granule Cell Layer. SGZ, Subgranular Zone. DG, Dentate Gyrus.

hippocampal sections showing cells labelled by CldU injections at P6 in WT and TNAP-/- mice treated with the P2X7R antagonist BBG or vehicle. Scale bar: 25 µm. (**D**) Total number of cells labelled by CldU in granule cell layer ($n \geq 3$ mice at P9 per genotype and treatment; sections ≥8 per mouse). (**E**) The granule cell layer was divided in 3 equal-sized regions or bins to make quantitative analysis of the distribution of CldU populations ($n \geq 3$ mice at P9 per genotype and treatment and sections ≥18 per mouse). (**F**) Representative immunofluorescence images of nuclei of CA3 pyramidal layer proximal to the dentate gyrus (CA3pDG, dotted line) stained with antibodies against Calbindin and DAPI dye showing axonal sprouting. Scale bar: 50 µm. (**G**) Quantification of the size of different dentate gyrus layers ($n \geq 4$ mice at P9 per genotype and treatment and sections ≥10 per mouse). (H) Quantification of the size of CA3pDG area ($n \geq 4$ mice at P9 per genotype and treatment; sections ≥10 per mouse). (**I**) Representative western blot images from the lysate of hippocampus from P9 WT and TNAP-/- mice treated with BBG. Graphs show quantification of the protein expression of VGLUT1, VGAT and PSD-95 ($n \geq 4$ mice at P9 per genotype and treatment). (**J**) Micrograph showing c-Fos immunoreactivity in the dentate gyrus of P9 WT and TNAP-/- mice treated with BBG, the specific antagonist of P2X7R. Black arrowheads indicate c-Fos positive cells. Scale bar: 200 µm. (**K**) Total number of c-Fos positive cells in granule cell layer ($n \geq 3$ mice at P9 per genotype and treatment; sections ≥10 per mouse). #$P < 0.06$, *$P < 0.05$, **$P < 0.01$ and ***$P < 0.001$ using one-way ANOVA followed by Tukeýs multiple comparison test. Data in bar graphs depict mean ± s.e.m. ML, Molecular layer. GCL, Granule Cell Layer. SGZ, Subgranular Zone. DG, Dentate Gyrus.

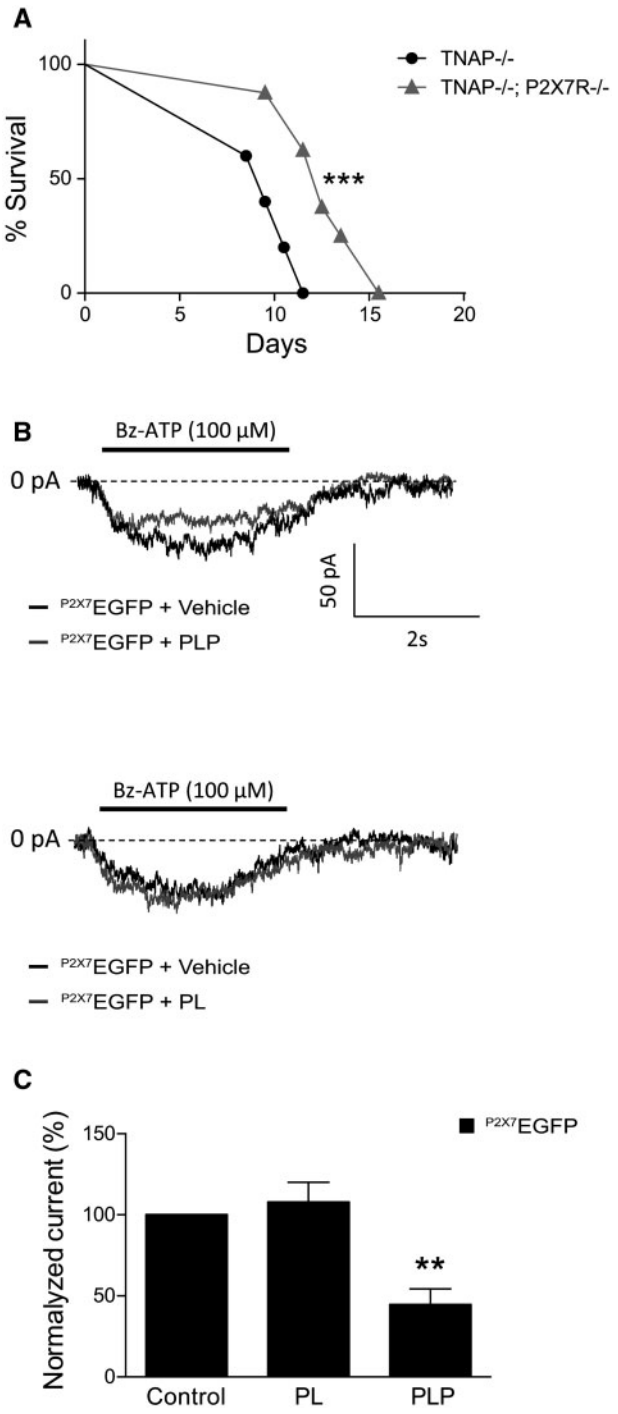

Figure 5. Selective knockdown and pharmacological inhibition of P2X7R increases the longevity of TNAP-/- mice. PLP but not PL decreases the response to Bz-ATP of ^{P2X7}EGFP cells from dentate gyrus. (**A**) Survival of TNAP-/- mice (black; $n = 5$) and TNAP-/-; P2X7R-/- mice (grey; $n = 10$). The log-rank test was used to compare survival between groups. (**B**) Representative patch-clamp recordings illustrating current responses to 100 μM Bz-ATP in EGFP-positive neurons placed in dentate gyrus from ^{P2X7}EGFP mice in the absence (vehicle) or the presence of 300 μM PLP or PL. (**C**) Graph indicates the quantification of patch-clamp recordings showing a significant decrease in the response to Bz-ATP when the slices are pre-treated with PLP ($n \geq 3$ mice at P9; cells ≥ 6 per mouse), but not with PL ($n \geq 3$ mice at P9; cells ≥ 5 per mouse). $^{**}P < 0.01$ between pharmacological pre-treatment and the corresponding vehicle using one-way ANOVA followed by Tukeýs multiple comparison test. Data in bar graphs depict mean ± s.e.m.

the seizures induced by SBI-425 were significantly longer in TNAP+/- mice than in WT mice (Figure 6G and Supplementary Material, Fig. S4C). It is noteworthy that while administration of ATP induced a significant increase in hippocampal levels of c-Fos mRNA and protein both in TNAP+/- and WT mice (Figure 6D and Supplementary Material. Fig. S4E), the TNAP antagonists only increased the levels of c-Fos in TNAP+/- mice but not in WT mice (Figure 6H and Supplementary Material, Fig. S4D).

Finally, to investigate the role of P2X7R in ATP- and levamisole-induced seizures, we treated TNAP+/- mice with levamisole in the absence or presence of the highly selective but rapidly reversible P2X7R antagonist A-438079. A-438079 pre-treatment reduced by almost half the number of mice suffering levamisole-induced seizures (from 70.0% to 39.1%), and decreased seizure duration (Figure 6F and G). Supporting that P2X7R is involved in seizures induced by ATP was obtained by the absence of any seizure activity in P2X7R-/- mice injected with ATP (Figure 6A–C). Altogether, these results demonstrate that increased brain levels of ATP by its direct administration or by TNAP inhibition induces seizures by activating P2X7R.

Discussion

The present study describes postnatal developmental defects in the hippocampus and neocortex in TNAP-/- mice. These alterations include delay in axonal growth, increased neurogenesis coupled with enhanced migration of newborn cells, dendritic spine loss and altered dendritic branching patterns, enhanced expression of VGLUT1, and increased c-Fos levels. These alterations have been previously described in other animal models that reproduce neonatal seizures (13,14) and in human neonates suffering seizures (36,37). However, it remains unclear whether these changes are a consequence or a cause of seizures, and if they contribute to susceptibility to seizures in adulthood (15). We found that these developmental defects in TNAP-/- mice were accompanied by a decrease in hippocampal and neocortical expression of P2X7R. Given that P2X7R-/- mice also show enhanced neurogenesis and alterations in dendritic and axonal branching patterns, but do not develop appreciable epileptic seizures, we propose that these morphological changes are a consequence rather than a cause of seizure activity in TNAP-/- mice.

We speculate that the reduced P2X7R levels in TNAP-deficient mice is a compensatory response that may offset the developmental defects detected in these mice, which may be caused by persistent activation of P2X7R, resulting from the high concentrations of ATP accumulated by its deficient hydrolysis. Supporting this hypothesis, we found that cerebral ecto-ATPase activity in TNAP-/- mice is lower than that detected in their corresponding WT littermates. In addition, we did not detect any compensatory transcriptional upregulation of other ectonucleotidases in TNAP-/- mice that could balance the lack of TNAP. This hypothesis is in agreement with previous studies performed in hippocampal-cultured neurons, where it was described that the increase on extracellular ATP levels induced by the inhibition or depletion of TNAP caused a persistent P2X7R activation that finally led to a decreased axonal growth (24). In line with this reasoning, we found that selective shRNAs against P2X7R reversed the deficient axonal growth profile detected in TNAP-/- mice at the first postnatal day. Although a reduction in the number of spines was detected in these mice, in contrast to the outcome expected if the deficient axonal growth is maintained over time, no significant reduction in the number of synaptic contact have been detected in TNAP-/- mice after

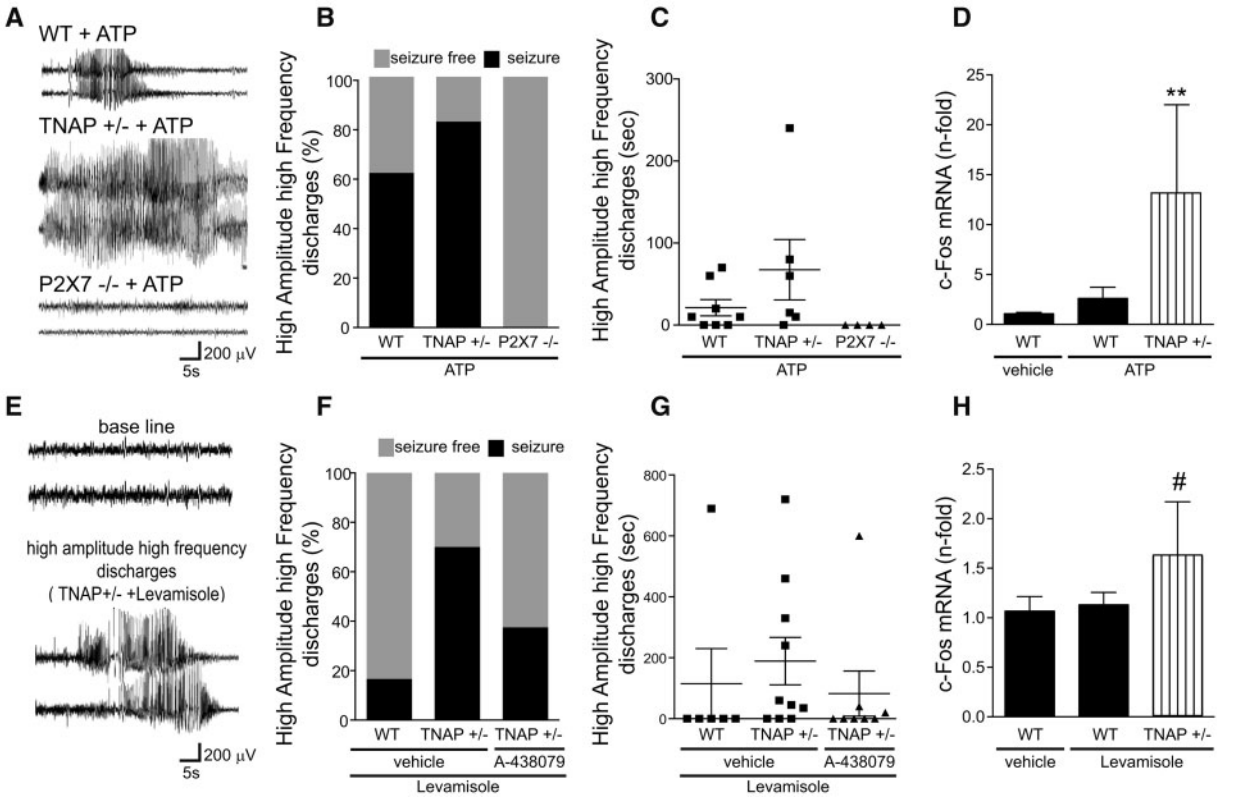

Figure 6. TNAP antagonists and ATP induce seizures by P2X7R activation. (**A**) Representative EEG spectrograms showing frequency and amplitude data during ATP-induce seizure in WT, TNAP+/- or P2X7R-/- mice. (**B**) Percentage of animals that suffer seizures after i.c.v. ATP administration ($n = 8$ WT mice at 2-3M months-old; $n = 6$ TNAP+/- mice at 2-3M months-old; $n = 4$ P2X7R-/- mice at 2-3M months-old). (**C**) Average duration of HAHFDs during seizure ($n = 8$ WT mice at 2-3M months-old; $n = 6$ TNAP+/- mice at 2-3M months-old; $n = 4$ P2X7R-/- mice at 2-3M months-old). (**D**) Levels of the activity-regulated gene c-Fos from ipsilateral hippocampus lysates 2 h after i.c.v. administration of ATP or the corresponding vehicle in WT or TNAP+/- animals ($n \geq 4$ mice at 2-3M months-old per genotype and treatment). (**E**) Representative EEG spectrograms showing frequency and amplitude data during Levamisole-induced seizure in TNAP+/- mice. (**F**) Percentage of animals that suffer seizures after i.c.v. Levamisole administration showing a protective effect of P2X7R antagonist A-438079 ($n = 6$ WT mice at 2-3M months-old treated with vehicle; $n = 10$ TNAP+/- mice at 2-3M months-old treated with vehicle; $n = 8$ TNAP+/- mice at 2-3M months-old treatment with A-438079) (**G**) Average duration of HAHFDs during seizure ($n = 6$ WT mice at 2-3M months-old treated with vehicle; $n = 10$ TNAP+/- mice at 2-3M months-old treated with vehicle; $n = 8$ TNAP+/- mice at 2-3M months-old treatment with A-438079). (**H**) Levels of the activity-regulated gene c-Fos from ipsilateral hippocampus lysates 2 h after i.c.v. administration of Levamisole or the corresponding vehicle ($n \geq 6$ mice per genotype and treatment). #$P < 0.06$ or **$P < 0.01$ between WT and TNAP+/- mice using one-way ANOVA followed by Tukey's multiple comparison test. Data in bar graphs depict mean ± s.e.m.

two weeks of life (20). Supporting the hypothesis that reduced P2X7R expression facilitates the establishment of synaptic contacts in TNAP-/- mice, we observed a progressive increase in levels of presynaptic markers that paralleled the decline in P2X7R expression. Besides, lower expression levels of PSD-95 detected in TNAP-/- mice compared to WT mice, a protein implicated in the stabilization of young synaptic contacts (38), suggest that synaptic contacts in WT mice are more mature than in TNAP-/- mice. Indeed, the ultrastructure study performed by electron microscopy revealed that the size of synaptic contacts is lower in TNAP-/- mice than in WT mice (20). Taken together, these findings suggest that hippocampal neurons in TNAP-/- mice undergo alterations in their developmental program that delay the establishment of synaptic contacts and may favour the persistence of immature neurons, which have been proposed to contribute to seizure generation (16).

Since the reduction in P2X7R levels appeared uniform in all neurons of GCL regardless of their stage of development, it is reasonable to think that the resulting consequences will affect all the events involved in neuronal differentiation. This is in agreement with observations in P2X7R-/- mice and with findings reported by other authors (24,26). We can suggest that the reduction of P2X7R expression in both neural precursors and immature neurons from GCL of DG in TNAP-/- mice is the responsible factor of the increase on neurogenesis and the axonal and dendritic sprouting detected in TNAP-/- mice. On the other hand, the deficient ATP hydrolysis in TNAP-/- mice might favour an abnormal activation frequency of the few presynaptic P2X7 receptors that still express mature neurons from GCL of DG. Since other authors have reported that P2X7R activation in hippocampal neurons induces presynaptic depolarization (30), it would reasonable to think that as a result of recurring presynaptic depolarizations, an abnormal neuronal hyper-excitability would be induced causing seizures that result in an increased neuronal c-Fos expression (39). In agreement with these hypotheses, it was reported that unlike WT mice, deficient P2X7R mice do not show an increased c-Fos expression in DG as a result of the enhanced neuronal activity after repeated stress exposures (40,41). In addition, this hypothesis also seems to agree with our previous findings demonstrating that pharmacological blockade of P2X7R attenuates seizure severity and neuronal death induced by intra-amygdala administration of KA (32,33). However, the mechanisms underlying the protective effects would be different in each model. Thereby, the protective effect of P2X7R blockers on seizures induced by KA is due to the fact that they prevent P2X7R activation by the ATP released by

activation of glutamate receptors sensitive to KA (32). Meanwhile, in TNAP-/- mice, the P2X7R activation would induce seizures and glutamate release (30), the latter in turn favoured by high levels of VGLUT1, leading to glutamate receptor activation that would enhance the pro-convulsant effect of ATP. These hypotheses are also supported by results obtained in P2X7R-deficient mice. In P2X7R-deficient mice, while KA administration still causes seizures, albeit less severe than in WT mice (32), ATP administration did not. Finally, the absence of seizure activity in either TNAP-/- mice treated with P2X7 antagonists or in mice lacking both TNAP and P2X7R, confirm that seizures and toxicity effects detected in TNAP-/- mice are triggered by activation of P2X7R. In agreement with this conclusion, the longevity of the mice lacking both TNAP and P2X7R was greater than in TNAP-/- mice.

Based on a recent study describing that P2X7R may be blocked by PLP (34), we sought to determine whether P2X7R plays a role in the beneficial effect of oral administration of PL in TNAP-/- mice (5,6). The absence of TNAP in blood cells and plasma prevents the dephosphorylation of PLP coming from the liver into PL, the form in which vit-B6 is transported through membranes, resulting in the accumulation of PLP in the blood. Consequently, the subsequent release of the vitamin, in the form of PLP, by the choroid plexus into the cerebrospinal fluid is also compromised (42). The decrease in cerebral PLP levels results in reduced neuronal levels of PL, which is an essential cofactor for cytosolic GABA synthesis. Because PL treatment rescues the reduction in GABA levels in TNAP-/- mice, it was initially postulated that seizure activity is caused by a deficiency in GABAergic innervation, which is unable to adequately balance the incipient excitatory neurotransmission (6). In support of this hypothesis, both functional alterations as a deficient maturation of the inhibitory GABAergic system has been linked with a higher susceptibility to develop seizures by human neonates. (16,43). Accordantly with these data, and considering the deficient cytosolic GABA synthesis that TNAP-/- mice have, it would be reasonable to think that they might develop some compensatory mechanism to balance this deficiency. However, our analysis did not provide any data to support this hypothesis, showing that TNAP-/-mice expressed similar VGAT brain levels than WT mice. Nevertheless, if we consider that PLP and not PL is capable to block P2X7R, the reduction of brain PLP levels in TNAP/- mice (6) may indicate that basal P2X7R inhibition is reduced in these mice. This would favour P2X7R activation and thus the hyperexcitability of hippocampal neurons, causing the convulsions.

Consistent with our observations in neonatal mice, activation of hippocampal P2X7R, induced either by direct administration of ATP or by pharmacological blockade of TNAP, also elicited seizures in adult mice. These results shed light on a novel potential molecular mechanism underlying the diazepam and lorazepam-resistant seizures induced in adult humans by oral ingestion of levamisole (9,10), and constitute an important addition to research into convulsions caused by the use of levamisole-adulterated cocaine (11,12). Our findings suggest that any factor that alters the expression or functionality of TNAP will increase susceptibility to seizures by altering brain levels of ATP. In support of this view, we observed that heterozygote TNAP+/- mice, which inherit only half the genetic load for this enzyme, are more likely to experience seizures than their WT littermates. Moreover, the fact that heterozygote mice apparently did not develop seizures at the neonatal stage (5,6), indicating that enzymatic TNAP activity, even this being as low as the expressed by heterozygous mice, is essential to regulate extracellular ATP levels in the brain.

In summary, here we demonstrate that TNAP plays a key role in postnatal neuronal development by controlling P2X7R. The absence or inhibition of TNAP at this stage results in apparent compensatory changes in the levels of neuronal P2X7R and enhances susceptibility to ATP-provoked seizures. In agreement with these findings, we also report that the beneficial effects of vit-B6 treatment are due, at least in part, to its ability to block P2X7R. Our results demonstrate for the first time that ATP is capable by itself to trigger seizures both in newborn and in adult mice via P2X7R activation.

Materials and Methods

Animals

All animal procedures were carried out at the Complutense University of Madrid, in compliance with National and European regulations (RD1201/2005; 86/609/CEE) following the guidelines of the International Council for the Laboratory Animal Science. All surgery was performed under isoflurane anaesthesia, and all efforts were made to minimize suffering. The morning of the day of the appearance of a vaginal plug was defined as E0.5.

P2X7R reporter mice (Tg [P2rx7-EGFP]FY174Gsat/Mmcd, stock 011959-UCD) expressing EGFP immediately downstream of the P2X7R promoter were obtained from the U.S. National Institutes of Health Mutant Mouse Regional Resource Centers and granted by Dr. M. Nedergaard (University of Rochester, Rochester, NY, U.S.A.). TNAP-/- mice were generated by the inactivation of the mouse *Akp2* gene, as previously described (4). P2X7R-/- mice were obtained from Pfizer (Groton, CT, USA), generated by (44). Genotyping was performed as indicated in Supplementary Material.

Infection with retrovirus at gestational stage. Dendritic branching and spine number analysis

At E14.5, pregnant C57BL/6 female mice were anaesthetized by continuous inhalation of Isoflurane (Baxter, Deerfield, US). The abdomen was opened and the uterine horns exposed. The retrovirus stock preparation containing 0.03% fast green was injected into one lateral ventricle of each embryo using a pulled glass micropipette. The wall and skin of the abdominal cavity were sutured and the embryos were allowed to develop normally until P9. Retroviral stock preparation was prepared as indicate in Supplementary Material.

The spine number and dendritic branching (number of primary, secondary and tertiary branches) of individual neurons of the somatosensory cortex or DG were measured with ImageJ and NeuronJ software in confocal reconstructions. Measu rements were only made on cortical neurons with the main apical process parallel to the plane of section contacting layer I, and with at least three basal processes.

BBG and CldU injections and cell counting

The specific P2X7R antagonist BBG (Sigma-Aldrich) was dissolved in PBS-DMSO 0.2% (5mg/mL) and was administered every 48h through intraperitoneal injections (45 mg/kg). Offspring coming from TNAP heterozygous crosses were treated with BBG from P1 to their death. In some cases, both TNAP-/- mice and WT mice treated with BBG were sacrificed at P9 to be analysed. For proliferation and migration experiments CldU (85 mg/kg,

Sigma-Aldrich) was injected 2 times at P6 and animals were sacrificed at P9.

Anatomically matched sections were selected from each mouse at P9, and CldU was detected by immune-fluorescence techniques as described in Supplementary Material. For proliferation studies, the number of CldU positive cells was counted in the GCL of the DG. While for migration assays, the total thickness of GCL was subdivided into 3 regions or bins of equal area, and the number of CldU positive cells was counted in each bin

Electrophysiological recordings in brain slices

Brain slices were prepared as indicated in the Supplementary Material. Drugs were applied onto the cell under investigation by means of a glass-pipette (3–5 μm tip diameter) connected to a pneumatic drug ejection system (PDES-02DX, NPI Elect ronic GmbH, Germany). Ligand-gated currents were evoked by the P2X7 receptor agonist, BzATP (2′(3′)-O-(4-Benzoylben zoyl) adenosine 5′-triphosphate 100 μM; 3 sec; Sigma Aldrich, Spain). When used, 300 μM PL (Sigma Aldrich, Spain), 300 μM PLP or 10 μM A438079 (3-[[5-(2, 3-dichlorophenyl)-1H-tetrazol-1- yl] methyl]pyridine hydrochloride) (Tocris Biosciences, Bristol, United Kingdom) were applied from a separate glass pipette 2 min before and during BzATP administration. Stock solutions of drugs were make freshly every day in the extracel lular saline, and the application pipettes were filled with the drugs solutions a few minutes before starting the experiments.

In vivo seizure induction and recording

First, WT or TNAP+/- mice were anaesthetized using isoflurane (3–5%) and maintained normothermic by means of a feedback-controlled heat blanket (Harvard Apparatus Ltd, Kent, United Kingdom). Mice were then placed in a stereotaxic frame, and three cortical skull-mounted EEG electrodes attached (Bilaney Consultants Ltd, Sevenoaks, United Kingdom). EEG was recorded using a Grass Comet XL digital EEG (Medivent Ltd, Lucan, Ireland) and quantified as indicated in the Supplementary Material. A guide cannula was affixed (coordinates from Bregma: AP = 0.4 mm; L = 0.95 mm) and the entire skull assembly fixed in place with dental cement. Baseline EEG was recorded for at least 10 min., and then an injection cannula was lowered through the guide cannula for i.c.v. injection of 2 μL vehicle (PBS) or specific P2X7R inhibitor 875 μM A438079 followed 10 min by an injection again through the cannula of 0.175M Levamisole; 54 mM SBI-425 (45) or 0.5M ATP (Sigma-Aldrich, Arklow, Ireland). Mice were killed 2h later and perfused with saline to remove intravascular blood components. Brains were either processed as described in the Supplementary Material to perform quantitative PCR, Immunohistochemistry, immunofluorescence or Western blot assays.

In utero electroporation, tissue processing, quantitative PCR, western blot, enzyme activity, immunohistoch emistry immunofluorescence, image acquisition and calcium studies

These are described in the Supplementary Material together with axonal length analysis, measurement of DG area and EGFP-positive cells counting.

Statistics

Unless otherwise stated data are shown as mean values ± standard error of the mean (s.e.m). The numbers of mice per group or genotype used in each experiment are annotated in the corresponding figure legends as n. All experiments shown were reproduced 3–5 times independently. Figures and statistical analyses were generated using GraphPad Prism 6 (GraphPad Software). Results were analysed by un-paired Students t-tests, ANOVA with Bonferroni post hoc or log-rank test. The statistical test used and P values are indicated in each figure legend. $P \leq 0.05$ was considered statistically significant. * $P \leq 0.05$, ** $P \leq 0.01$, *** $P \leq 0.001$ and ns, not significant.

Supplementary Material

Supplementary Material is available at *HMG* online.

Acknowledgements

We thank Dr. M. Nieto for critical reading of the manuscript and for the anti-Cux1 and anti-Ctip2 antibodies, Dr. M. Nedergaard for P2X7R reporter mice, Prof. Fred H. Gage for EGFP-expressing retrovirus and Dr. T. Poderoso for her technical assistance.

Conflict of Interest Statement. None declared.

Funding

This work was supported by funding from the Spanish Ministry of Science and Education (BFU2012-31195 to MDH; BFU-2014-53654-P to M.T.M-P; BFU2011-26253 to A.R.A), Universidad Complutense de Madrid (UCM)-Santander Central Hispano Bank (911585-670 to M.D-H.), Fundación Marcelino Botín (to M.T.M-P), Science Foundation Ireland (13/SIRG/2098, 12/RC/2272), Health Research Board Ireland (HRA-POR/2010/123, HRA-POR/2012/56, HRA-POR/2011/41) and grant DE12889 (to J.L.M.) from the National Institute of Dental and Craniofacial Research (NIDCR), National Institutes of Health (NIH), USA. A.S-S and C.M-F. are hired by BFU2012-31195 grant, and L.D.G. has a UCM predoctoral fellowship supervised by M.D-H. Funding to pay the Open Access publication charges for this article was provided by the Spanish Ministry of Science and Education.

References

1. Millan, J.L. (2006) Alkaline Phosphatases: Structure, substrate specificity and functional relatedness to other members of a large superfamily of enzymes. *Purinergic. Signal*, **2**, 335–341.
2. Narisawa, S., Hasegawa, H., Watanabe, K. and Millan, J.L. (1994) Stage-specific expression of alkaline phosphatase during neural development in the mouse. *Dev. Dyn.*, **201**, 227–235.
3. Whyte, M.P., Zhang, F., Wenkert, D., McAlister, W.H., Mack, K.E., Benigno, M.C., Coburn, S.P., Wagy, S., Griffin, D.M., Ericson, K.L., *et al.* (2015) Hypophosphatasia: validation and expansion of the clinical nosology for children from 25 years experience with 173 pediatric patients. *Bone*, **75**, 229–239.
4. Narisawa, S., Frohlander, N. and Millan, J.L. (1997) Inactivation of two mouse alkaline phosphatase genes and establishment of a model of infantile hypophosphatasia. *Dev. Dyn.*, **208**, 432–446.

5. Narisawa, S., Wennberg, C. and Millan, J.L. (2001) Abnormal vitamin B6 metabolism in alkaline phosphatase knock-out mice causes multiple abnormalities, but not the impaired bone mineralization. *J. Pathol.*, **193**, 125–133.
6. Waymire, K.G., Mahuren, J.D., Jaje, J.M., Guilarte, T.R., Coburn, S.P. and MacGregor, G.R. (1995) Mice lacking tissue non-specific alkaline phosphatase die from seizures due to defective metabolism of vitamin B-6. *Nat. Genet.*, **11**, 45–51.
7. Balasubramaniam, S., Bowling, F., Carpenter, K., Earl, J., Chaitow, J., Pitt, J., Mornet, E., Sillence, D. and Ellaway, C. (2010) Perinatal hypophosphatasia presenting as neonatal epileptic encephalopathy with abnormal neurotransmitter metabolism secondary to reduced co-factor pyridoxal-5'-phosphate availability. *J. Inherit. Metab. Dis.*, **33 Suppl 3**, S25–S33.
8. Baumgartner-Sigl, S., Haberlandt, E., Mumm, S., Scholl-Burgi, S., Sergi, C., Ryan, L., Ericson, K.L., Whyte, M.P. and Hogler, W. (2007) Pyridoxine-responsive seizures as the first symptom of infantile hypophosphatasia caused by two novel missense mutations (c.677T>C, p.M226T; c.1112C>T, p.T371I) of the tissue-nonspecific alkaline phosphatase gene. *Bone*, **40**, 1655–1661.
9. Aberastury, M.N., Silva, W.H., Vaccarezza, M.M., Maxit, C. and Agosta, G. (2011) Epilepsia partialis continua associated with levamisole. *Pediatr. Neurol.*, **44**, 385–388.
10. Galassi, G., Tassone, G., Sintini, M., Spagnoli, M., Bertolani, L. and Mavilla, L. (1996) 5-Fluorouracil- and levamisole-associated multifocal leukoencephalopathy. *Eur. Neurol.*, **36**, 244–246.
11. Shea, J.L. (2013) Bioanalytical methods for quantitation of levamisole, a widespread cocaine adulterant. *Clin. Chem. Lab. Med.*, **51**, 205–212.
12. Sordo, L., Indave, B.I., Degenhardt, L., Barrio, G., Kaye, S., Ruiz-Perez, I. and Bravo, M.J. (2013) A systematic review of evidence on the association between cocaine use and seizures. *Drug Alcohol Depend.*, **133**, 795–804.
13. Jiang, M., Lee, C.L., Smith, K.L. and Swann, J.W. (1998) Spine loss and other persistent alterations of hippocampal pyramidal cell dendrites in a model of early-onset epilepsy. *J. Neurosci.*, **18**, 8356–8368.,
14. Holmes, G.L., Gairsa, J.L., Chevassus-Au-Louis, N. and Ben-Ari, Y. (1998) Consequences of neonatal seizures in the rat: morphological and behavioral effects. *Ann. Neurol.*, **44**, 845–857.
15. Friedman, L. and Hu, S. (2014) Early-life seizures in predisposing neuronal preconditioning: a critical review. *Life Sci.*, **94**, 92–98.
16. Nardou, R., Ferrari, D.C. and Ben-Ari, Y. (2013) Mechanisms and effects of seizures in the immature brain. *Semin. Fetal Neonatal Med.*, **18**, 175–184.
17. Langer, D., Ikehara, Y., Takebayashi, H., Hawkes, R. and Zimmermann, H. (2007) The ectonucleotidases alkaline phosphatase and nucleoside triphosphate diphosphohydrolase 2 are associated with subsets of progenitor cell populations in the mouse embryonic, postnatal and adult neurogenic zones. *Neuroscience*, **150**, 863–879.
18. Kermer, V., Ritter, M., Albuquerque, B., Leib, C., Stanke, M. and Zimmermann, H. (2010) Knockdown of tissue nonspecific alkaline phosphatase impairs neural stem cell proliferation and differentiation. *Neurosci. Lett.*, **485**, 208–211.
19. Negyessy, L., Xiao, J., Kantor, O., Kovacs, G.G., Palkovits, M., Doczi, T.P., Renaud, L., Baksa, G., Glasz, T., Ashaber, M., *et al.* (2011) Layer-specific activity of tissue non-specific alkaline phosphatase in the human neocortex. *Neuroscience*, **172**, 406–418.
20. Hanics, J., Barna, J., Xiao, J., Millan, J.L., Fonta, C. and Negyessy, L. (2012) Ablation of TNAP function compromises myelination and synaptogenesis in the mouse brain. *Cell Tissue Res.*, **349**, 459–471.
21. Burnstock, G., Fredholm, B.B. and Verkhratsky, A. (2011) Adenosine and ATP receptors in the brain. *Curr. Top. Med. Chem.*, **11**, 973–1011.
22. Zimmermann, H., Zebisch, M. and Strater, N. (2012) Cellular function and molecular structure of ecto-nucleotidases. *Purinergic Signal*, **8**, 437–502.
23. Diaz-Hernandez, M., Pintor, J. and Miras-Portugal, M.T. (2000) Modulation of the dinucleotide receptor present in rat midbrain synaptosomes by adenosine and ATP. *Br. J. Pharmacol.*, **130**, 434–440.
24. Diez-Zaera, M., Diaz-Hernandez, J.I., Hernandez-Alvarez, E., Zimmermann, H., Diaz-Hernandez, M. and Miras-Portugal, M.T. (2011) Tissue-nonspecific alkaline phosphatase promotes axonal growth of hippocampal neurons. *Mol. Biol. Cell*, **22**, 1014–1024.
25. Sperlagh, B. and Illes, P. (2014) P2X7 receptor: an emerging target in central nervous system diseases. *Trends Pharmacol. Sci.*, **35**, 537–547.
26. Csolle, C., Baranyi, M., Zsilla, G., Kittel, A., Goloncser, F., Illes, P., Papp, E., Vizi, E.S. and Sperlagh, B. (2013) Neurochemical Changes in the Mouse Hippocampus Underlying the Antidepressant Effect of Genetic Deletion of P2X7 Receptors. *PLoS One*, **8**, e66547.
27. Gomez-Villafuertes, R., del Puerto, A., Diaz-Hernandez, M., Bustillo, D., Diaz-Hernandez, J.I., Huerta, P.G., Artalejo, A.R., Garrido, J.J. and Miras-Portugal, M.T. (2009) Ca2+/calmodulin-dependent kinase II signalling cascade mediates P2X7 receptor-dependent inhibition of neuritogenesis in neuroblastoma cells. *Febs J.*, **276**, 5307–5325.,
28. Deuchars, S.A., Atkinson, L., Brooke, R.E., Musa, H., Milligan, C.J., Batten, T.F., Buckley, N.J., Parson, S.H. and Deuchars, J. (2001) Neuronal P2X7 receptors are targeted to presynaptic terminals in the central and peripheral nervous systems. *J. Neurosci.*, **21**, 7143–7152.,
29. Sperlagh, B., Kofalvi, A., Deuchars, J., Atkinson, L., Milligan, C.J., Buckley, N.J. and Vizi, E.S. (2002) Involvement of P2X7 receptors in the regulation of neurotransmitter release in the rat hippocampus. *J. Neurochem.*, **81**, 1196–1211.
30. Cho, J.H., Choi, I.S. and Jang, I.S. (2010) P2X7 receptors enhance glutamate release in hippocampal hilar neurons. *Neuroreport*, **21**, 865–870.
31. Khakpay, R., Polster, D., Koles, L., Skorinkin, A., Szabo, B., Wirkner, K. and Illes, P. (2010) Potentiation of the glutamatergic synaptic input to rat locus coeruleus neurons by P2X7 receptors. *Purinergic Signal*, **6**, 349–359.
32. Engel, T., Gomez-Villafuertes, R., Tanaka, K., Mesuret, G., Sanz-Rodriguez, A., Garcia-Huerta, P., Miras-Portugal, M.T., Henshall, D.C. and Diaz-Hernandez, M. (2012) Seizure suppression and neuroprotection by targeting the purinergic P2X7 receptor during status epilepticus in mice. *Faseb J.*, **26**, 1616–1628.
33. Mesuret, G., Engel, T., Hessel, E.V., Sanz-Rodriguez, A., Jimenez-Pacheco, A., Miras-Portugal, M.T., Diaz-Hernandez, M. and Henshall, D.C. (2014) P2X7 receptor inhibition interrupts the progression of seizures in immature rats and reduces hippocampal damage. *CNS Neurosci. Ther.*, **20**, 556–564.
34. Theriault, O., Poulin, H., Thomas, G.R., Friesen, A.D., Al-Shaqha, W.A. and Chahine, M. (2014) Pyridoxal-5'-

phosphate (MC-1), a vitamin B6 derivative, inhibits expressed P2X receptors. *Can. J. Physiol. Pharmacol.*, **92**, 189–196.
35. Liu, J., Nam, H.K., Campbell, C., Gasque, K.C., Millan, J.L. and Hatch, N.E. (2014) Tissue-nonspecific alkaline phosphatase deficiency causes abnormal craniofacial bone development in the Alpl(-/-) mouse model of infantile hypophosphatasia. *Bone*, **67**, 81–94.
36. Catala, I., Ferrer, I., Galofre, E. and Fabregues, I. (1988) Decreased numbers of dendritic spines on cortical pyramidal neurons in dementia. A quantitative Golgi study on biopsy samples. *Hum. Neurobiol.*, **6**, 255–259.
37. Houser, C.R., Miyashiro, J.E., Swartz, B.E., Walsh, G.O., Rich, J.R. and Delgado-Escueta, A.V. (1990) Altered patterns of dynorphin immunoreactivity suggest mossy fiber reorganization in human hippocampal epilepsy. *J. Neurosci.*, **10**, 267–282.
38. Taft, C.E. and Turrigiano, G.G. (2014) PSD-95 promotes the stabilization of young synaptic contacts. *Philos Tran. R. Soc. Lond. B. Biol. Sci.*, **369**, 20130134.
39. Morgan, J.I., Cohen, D.R., Hempstead, J.L. and Curran, T. (1987) Mapping patterns of c-fos expression in the central nervous system after seizure. *Science*, **237**, 192–197.
40. Boucher, A.A., Arnold, J.C., Hunt, G.E., Spiro, A., Spencer, J., Brown, C., McGregor, I.S., Bennett, M.R. and Kassiou, M. (2011) Resilience and reduced c-Fos expression in P2X7 receptor knockout mice exposed to repeated forced swim test. *Neuroscience*, **189**, 170–177.
41. Labrousse, V.F., Costes, L., Aubert, A., Darnaudery, M., Ferreira, G., Amedee, T. and Laye, S. (2009) Impaired interleukin-1beta and c-Fos expression in the hippocampus is associated with a spatial memory deficit in P2X(7) receptor-deficient mice. *PLoS One*, **4**, e6006.
42. Spector, R. and Johanson, C.E. (2007) Vitamin transport and homeostasis in mammalian brain: focus on Vitamins B and E. *J. Neurochem.*, **103**, 425–438.
43. Treiman, D.M. (2001) GABAergic mechanisms in epilepsy. *Epilepsia*, **42 Suppl 3**, 8–12.
44. Solle, M., Labasi, J., Perregaux, D.G., Stam, E., Petrushova, N., Koller, B.H., Griffiths, R.J. and Gabel, C.A. (2001) Altered cytokine production in mice lacking P2X(7) receptors. *J. Biol. Chem.*, **276**, 125–132.
45. Sheen, C.R., Kuss, P., Narisawa, S., Yadav, M.C., Nigro, J., Wang, W., Chhea, T.N., Sergienko, E.A., Kapoor, K., Jackson, M.R., *et al.* (2015) Pathophysiological role of vascular smooth muscle alkaline phosphatase in medial artery calcification. *J. Bone Miner. Res.*, **30**, 824–836.